Hyperfine structure of transition metal defects in SiC

Benedikt Tissot[*] and Guido Burkard[†]
Department of Physics, University of Konstanz, D-78457 Konstanz, Germany

(Received 16 April 2021; accepted 22 July 2021; published 5 August 2021)

Transition metal (TM) defects in silicon carbide (SiC) are a promising platform in quantum technology, especially because some TM defects emit in one of the telecom bands. We develop a theory for the interaction of an active electron in the D shell of a TM defect in SiC with the TM nuclear spin and derive the effective hyperfine tensor within the Kramers doublets formed by the spin-orbit coupling. Based on our theory we discuss the possibility to exchange the nuclear and electron states with potential applications for nuclear spin manipulation and long-lived nuclear-spin based-quantum memories.

DOI: 10.1103/PhysRevB.104.064102

I. INTRODUCTION

For several applications in quantum technology, such as quantum networks, memories, emitters, and many more [1–4], a quantum system needs to be coherently controlled and isolated from unwanted noise at the same time. Hybrid quantum systems [5–7], consisting of a part that can couple strongly to external fields as well as a part that is better shielded from its environment, are promising platforms to fulfill this requirement. In these systems one can benefit from short gate times of one quantum system as well as long coherence times of the other. A much studied system of this type is the nitrogen vacancy center in diamond with its neighboring nuclear spins [8–16] (and Refs. [17,18] for reviews).

Transition metal (TM) defects in silicon carbide (SiC) constitute a similar family of systems that have the benefit of being based on a well established host material as well as having accessible transitions in the telecommunication bands [19–23]. Recent studies made the first steps towards control of nuclear spins via transition metal defects in SiC [22]. While these results are highly promising, a complete theoretical framework is still needed. In this paper, we derive a model of the hyperfine coupling based on the underlying symmetry properties and relevant orbital configuration of the defect in the crystal, explaining the experimental data and leading to additional insights. In particular we derive a sensible form of the interaction of the defect nuclear spin with the spin and orbital angular momentum of the active electron as well as their combined interaction with external fields.

The prime examples for TM defects in SiC are created by neutral vanadium (V) and positively charged molybdenum (Mo) atoms substituting a Si atom in 6H- or 4H-SiC [19–25]. These defects have one active electron in the atomic D shell and are invariant under the transformations of the C_{3v} point group imposed by the crystal structure surrounding the defect, leading to the electronic level structure shown in Fig. 1(a). While the interaction with the nuclear spins of neighboring C and Si isotopes with nonzero nuclear spins is possible, the presence of such nonzero spin isotopes as a nearest neighbor is fairly improbable, because their natural abundances are about 1% for ^{13}C (spin 1/2) and 5% for ^{29}Si (spin 1/2) [26] and the abundance can be further reduced by using isotopically purified SiC [27,28]. Here, we therefore concentrate on the interaction with the TM nuclear spin. The nuclear spin for the most common V isotope is $I = 7/2$ (>99%) and $I = 5/2$ for about 25% of the stable Mo isotopes and $I = 0$ for the remaining isotopes of Mo [26,29].

II. MODEL

In order to model the coupling between the electron and nuclear spin in a TM defect in SiC, we start from the full Hamiltonian

$$H = H_{\mathrm{el}} + H_d + H_{\mathrm{hf}} + H_q + H_{z,\mathrm{nuc}} + H_{d,\mathrm{nuc}}. \tag{1}$$

The static electronic Hamiltonian H_{el} describes the electronic orbital and spin degrees of freedom including the Zeeman term H_z for the interaction with a static magnetic field. The electronic driving Hamiltonian H_d models the interaction of the electron with an oscillating (electric or magnetic) field, e.g., for optical driving it is given by the electric dipole coupling $H_d^E = e\vec{E}(t)\cdot\vec{r}$. The remaining terms are the focus of this work; they incorporate the nuclear spin of the TM and its interaction with the electron as well as external fields.

We discussed the first two terms $H_{\mathrm{el}} + H_d$ and the selection rules between electronic states in detail in Ref. [30]; in the following we give a summary of the relevant properties with additional information in Appendix A. While the state describing the active electron shows the transformation properties of a d orbital, due to effects such as the Jahn-Teller effect and covalency [23,31,32], there can be an admixture of other orbitals. The Wigner-Eckart theorem [13,33] enables us to absorb these effects as well as the radial part of the wave function in reduced matrix elements. Here, we treat reduced matrix elements as parameters that can be obtained experimentally or via *ab initio* calculations.

The structure of the electronic system is given by five Kramers doublets (KD), pairs of states related by time-

[*]benedikt.tissot@uni-konstanz.de
[†]guido.burkard@uni-konstanz.de

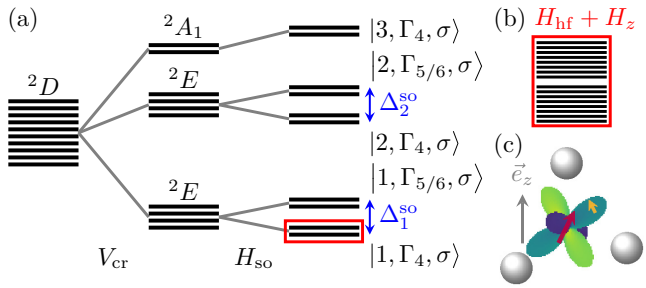

FIG. 1. Spin-orbit (a) and hyperfine (b) energy level structure of the active electron bound to the transition metal (TM) defect. The artistic illustration (c) shows the electron with spin-1/2 (yellow arrow) occupying a D shell (green and violet) which is split by the C_{3v} symmetric crystal potential V_{cr}, arising from the surrounding crystal atoms, into two orbital doublets E and an orbital singlet A_1 (a). The white balls correspond to the nearest-neighbor atoms obeying T_d symmetry which is further reduced to C_{3v} by the atoms in the outer coordination shells (not shown). The spin-orbit interaction H_{so} further splits each of the orbital doublets into two Kramers doublets (KDs), leading to the final spin-orbit structure given by five KDs. These KDs are then further split into hyperfine levels, due to the interaction with the TM nuclear spin [purple arrow in (c)], shown in (b) for the KD in the red frame.

reversal symmetry [34], with distinct zero-field energies $E_{j,\Gamma_{5/6}}, E_{i,\Gamma_4}$, where we label the orbital configuration with $j = 1, 2$ and $i = 1, 2, 3$ and the irreducible representation (irrep) of C_{3v} pertaining to the KD with Γ_γ [30]. The time-reversal symmetry protects KDs from coupling via operators that are invariant under time reversal. But they can be split via a static magnetic field $\vec{B}$ due to the Zeeman term.

Matrix elements mixing the KDs with the same orbital origin due to a static magnetic field perpendicular to the crystal axis are suppressed by the spin-orbit splitting

$$\Delta_j^{so} = E_{j,\Gamma_{5/6}} - E_{j,\Gamma_4} \tag{2}$$

and therefore can be neglected for small fields $|\vec{B}_\perp| \ll \min_{j=1,2} |\Delta_j^{so}|/\mu_B g_s$, with the Bohr magneton μ_B. Typically, the crystal potential is sufficiently large to neglect the coupling between states originating from different atomic orbitals due to a static magnetic field.

In the following we neglect the mixing of the KDs due to the static magnetic field, enabling the description of the KDs as separate pseudospin systems, described by the Hamiltonians

$$H_{i,\Gamma_\gamma}^{KD} = E_{i,\Gamma_\gamma} + \frac{\mu_B}{2}\vec{B}\mathbf{g}_{i,\Gamma_\gamma}\vec{\sigma}_{i,\Gamma_\gamma}, \tag{3}$$

with the vector of Pauli operators $\vec{\sigma}_{i,\Gamma_\gamma}$ acting between the KD states $|i, \Gamma_\gamma, \uparrow\rangle$ and $|i, \Gamma_\gamma, \downarrow\rangle$ [see Eqs. (B13)–(B15)] and the pseudospin g-tensor $\mathbf{g}$. For all KDs $\mathbf{g}_{i,\Gamma_\gamma}$ is diagonal: For the $\Gamma_{5/6}$ KDs only $g^{\parallel}_{i,\Gamma_{5/6}} \neq 0$; for the Γ_4 KDs with $j = 1, 2$ one finds [30] $g^{\parallel}_{j,\Gamma_4} \gg g^{\perp}_{j,\Gamma_4}$ if the spin-orbit coupling strength is much smaller than the crystal level spacing. Here we choose the crystal axis parallel to the z axis, i.e., $g^{\parallel}_{j,\Gamma_\gamma}$ couples B_z to $\sigma^z_{i,\Gamma_\gamma}$. Using the projection onto the subspace of the KD P_{i,Γ_γ} we can combine these Hamiltonians to obtain the complete effective electronic Hamiltonian $H_{el}^{eff} = \sum_{i,\Gamma_\gamma} P_{i,\Gamma_\gamma} H_{i,\Gamma_\gamma}^{KD} P_{i,\Gamma_\gamma}$.

Now we incorporate the interaction between the electron and the nucleus in Eq. (1). We take the Fermi contact and anisotropic hyperfine interaction, as well as the interaction of the orbital angular momentum with the nuclear spin, into account. The total hyperfine Hamiltonian [35–38] can be written as

$$\begin{aligned} H_{hf} &= H_{FC} + H_{ahf} + H_{orb} \\ &= \{a_{FC}\vec{S} + a[\vec{S} - 3(\vec{e}_r \cdot \vec{S}) \cdot \vec{e}_r - \vec{L}]\} \cdot \vec{I}, \end{aligned} \tag{4}$$

with the electron (nuclear) spin $\vec{S}$ ($\vec{I}$) and orbital angular momentum $\vec{L}$ in units of the reduced Planck constant $\hbar$, the electron direction operator $\vec{e}_r = \vec{r}/|\vec{r}|$, and the anisotropic hyperfine and Fermi contact coupling strengths $a = g_s\mu_B\mu_0 g_N\mu_N/4\pi r^3$ and $a_{FC} = -2g_s\mu_B\mu_0 g_N\mu_N\delta(r)/3$, with the vacuum permeability μ_0, the free electron and nuclear g factors $g_s = 2$ and g_N, and the nuclear magneton μ_N. The anisotropic coupling strength depends on the electronic state via $1/r^3$ while the Fermi contact interaction depends on the spin polarization density at the position of the nucleus denoted using the delta distribution $\delta(r)$. The active electron is mainly localized in a D shell but core-shell polarization can still lead to a relevant Fermi contact interaction, which is known for TM complexes [39–42]. In a simplified manner one might understand this as some form of mixing with s orbitals.

In addition to the dipolar interaction we also incorporate the nuclear quadrupolar term [36–38]

$$H_q = \frac{eQ}{6I(2I-1)} \sum_{i,j=x,y,z} \frac{\partial^2 V}{\partial i \partial j}\left[\frac{3}{2}(I_i I_j + I_j I_i) - \delta_{ij}\vec{I}^2\right], \tag{5}$$

describing the coupling between the nucleus and the (anisotropic) electric field gradient $\partial^2 V/\partial i\partial j$ at the origin, due to the nuclear quadrupole moment Q. Assuming that external fields do not vary on the scale of the nucleus and considering that a potential with cubic symmetry does not contribute to the quadrupole interaction, only the gradient of the crystal potential that reduces T_d symmetry to C_{3v} and the charge distribution of the orbital state of the active electron contribute to this term.

The nuclear spin can couple to external magnetic fields described by the nuclear Zeeman Hamiltonian

$$H_{z,nuc} = \mu_N g_N \vec{I} \cdot \vec{B}, \tag{6}$$

and the corresponding driving $H_{d,nuc}$ term for oscillating magnetic fields. These terms are small in comparison to the KD Zeeman part $|\mu_N g_N| \ll g^{\parallel}_{i,\Gamma_\gamma}\mu_B$ [22,25,43] and diagonal for $\vec{B}$ parallel to the crystal axis.

III. RESULTS

We derive the minimal set of nonzero matrix elements of (mixed) square components of $\vec{e}_r$ found by expanding Eq. (4) in the eigenbasis of the crystal potential using the Wigner-Eckart theorem. Then we transform the resulting Hamiltonian to the eigenbasis of the electronic Hamiltonian (for $B_x = B_y = 0$); the details of this are given in Appendix B. As we did for the mixing due to external fields we neglect off-diagonal blocks between different orbital configurations i due to the

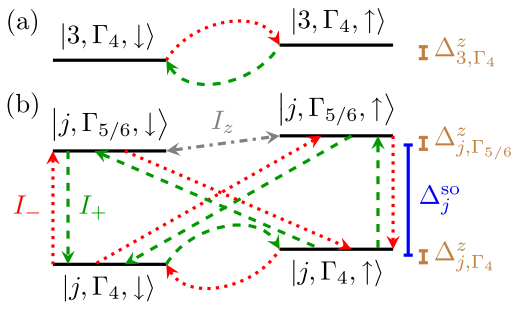

FIG. 2. Nonzero matrix elements of $H^{\text{eff}}_{\text{hf}}$ between states of two KDs originating from the same orbital doublet. The black lines correspond to the electronic pseudospin states becoming multiplets when taking the nuclear spin into account. The matrix elements between states of the same Γ_4 KD are proportional to $I_\pm$ (red dotted and green dashed arrows) while they are proportional to I_z (gray dash-dotted arrow) between states of the $\Gamma_{5/6}$ KDs. Inside the KDs the (off-diagonal) hyperfine interaction competes with the Zeeman splitting (brown). The matrix elements between states of the different KDs of the same orbital doublet are proportional to $I_\pm$ and suppressed by the spin-orbit splitting Δ^{so}_j (blue).

crystal field splitting. We find for the effective hyperfine Hamiltonians inside the KDs,

$$H^{\text{hf}}_{j,\Gamma_{5/6}} = \frac{1}{2}\left(a^{\parallel}_{j,\Gamma_{5/6}}\sigma^z_{j,\Gamma_{5/6}} + a^{\perp}_{j,\Gamma_{5/6}}\sigma^x_{j,\Gamma_{5/6}}\right)I_z, \tag{7}$$

$$H^{\text{hf}}_{j,\Gamma_4} = \frac{a^{\parallel}_{j,\Gamma_4}}{2}\sigma^z_{j,\Gamma_4}I_z + \frac{a^{\perp}_{j,\Gamma_4}}{4}(\sigma^+_{j,\Gamma_4}I_+ + \sigma^-_{j,\Gamma_4}I_-), \tag{8}$$

$$H^{\text{hf}}_{3,\Gamma_4} = \frac{a^{\parallel}_{3,\Gamma_4}}{2}\sigma^z_{3,\Gamma_4}I_z + \frac{a^{\perp}_{3,\Gamma_4}}{4}(\sigma^+_{3,\Gamma_4}I_- + \sigma^-_{3,\Gamma_4}I_+), \tag{9}$$

for $j = 1, 2$ and using the pseudospin $\sigma^{\pm}_{i,\Gamma_\gamma} = \sigma^x_{i,\Gamma_\gamma} \pm \mathrm{i}\sigma^y_{i,\Gamma_\gamma}$ as well as nuclear $I_\pm = I_x \pm \mathrm{i}I_y$ ladder operators. A similar form of the hyperfine coupling tensors was found in Ref. [44] for D_{3h} only using the transformation properties of the pseudospin. Here we begin at the orbital level to be able to link the form of the hyperfine coupling to the orbital configuration of the KD. The block-diagonal part of the total effective hyperfine Hamiltonian can thus be written as $H_{\text{hf,bd}} = \sum_{i,\Gamma_\gamma} P_{i,\Gamma_\gamma} H^{\text{hf}}_{i,\Gamma_\gamma} P_{i,\Gamma_\gamma}$. The terms mixing the KDs of the same orbital doublet are

$$H_{\text{hf,od}} = \sum_{j,\sigma}\big(a_{j,c\sigma}\,|j,\Gamma_{5/6},\sigma\rangle\,\langle j,\Gamma_4,\sigma|\,I_\sigma + a_{j,f}\,|j,\Gamma_{5/6},\sigma\rangle\,\langle j,\Gamma_4,-\sigma|\,I_{-\sigma} + \text{H.c.}\big), \tag{10}$$

where $\sigma = \pm 1 = \uparrow, \downarrow$. Combined this leads to the effective hyperfine Hamiltonian $H^{\text{eff}}_{\text{hf}} = H_{\text{hf,bd}} + H_{\text{hf,od}}$. The resulting coupling structure is depicted in Fig. 2.

To treat the quadrupole term (5) inside an orbital subspace we use that it only includes time reversal symmetric electronic operators and furthermore C_{3v} fulfills an axial symmetry (here around the z axis). The first implies that the states of one KD cannot be mixed by the coupling, the second that only the anisotropy component along the z axis contributes, i.e.

$$H^q_{j,\Gamma_\gamma} = q_{j,\Gamma_\gamma}\left[3I_z^2 - I(I+1)\right], \tag{11}$$

with $q_{j,\Gamma_\gamma} = eQ\,\langle j,\Gamma_\gamma,\sigma|\partial^2 V_{cr}/\partial z^2|j,\Gamma_\gamma,\sigma\rangle\,/6I(2I-1)$. Because there are no electron spin operators in this Hamiltonian, the electronic operator part is even proportional to unity in the whole orbital subspace apart from corrections due to the spin-orbit coupling. Therefore we neglect the part of the quadrupole interaction mixing the KDs solely stemming from the spin-orbit mixing of the states.

Combining the effective spin-orbit (3), hyperfine (7)–(10), nuclear quadrupole $H^{\text{eff}}_q = \sum_{i,\Gamma_\gamma} P_{i,\Gamma_\gamma} H^{\text{q}}_{i,\Gamma_\gamma} P_{i,\Gamma_\gamma}$, and nuclear Zeeman (6) contributions, we summarize our first main result as

$$H_{\text{eff}} = H^{\text{eff}}_{\text{el}} + H^{\text{eff}}_{\text{hf}} + H^{\text{eff}}_q + H_{z,\text{nuc}}. \tag{12}$$

The immediate implications of Eq. (12) are given by its projection on the KDs, corresponding to the effective description for negligible inter-KD mixing $|a_{j,c}|, |a_{j,f}| \ll |\,|\Delta^{so}_j| - \sum_\gamma \mu_B\,|g^{\parallel}_{i,\Gamma_\gamma}B_\parallel|\,/2|$. The importance of this is further underlined considering measurements by Wolfowicz *et al.* [22] where the hyperfine coupling strength is at least two orders of magnitude smaller than the spin-orbit splitting in all V defects in 4H- and 6H-SiC for the ground state ($j = 1$).

A. Discussion of the Hyperfine Tensor

We now discuss the projection of Eq. (12) onto the KDs in more detail. The effective hyperfine coupling in the $|3,\Gamma_4,\sigma\rangle$ KD is the most similar to the simple diagonal dipolar coupling to the nuclear spin, because the crystal potential does not mix the orbital singlet ($m = 0$) state with the remaining orbital states and the spin-orbit coupling vanishes in first order in the orbital singlet. Additionally, the form of the symmetry allowed part of the anisotropic hyperfine tensor in this case also agrees with that of the ^{14}N NV$^-$ center which has the same symmetry but comprises spins $S = I = 1$ [8,12,15].

The KDs originating from the orbital doublets deviate significantly from this form, because the pseudospin states have a different spin and orbital wave function, due to the interplay of the crystal potential and the spin-orbit coupling. This leads to the (pseudo)spin-nonconserving coupling, i.e., the nondiagonal coupling $\sigma^x_{j,\Gamma_{5/6}}I_z$ of the $\Gamma_{5/6}$ KDs as well as the $\sigma^{+(-)}_{j,\Gamma_4}I_{+(-)}$ coupling of the Γ_4 KDs for $j = 1, 2$, see Fig. 2. Furthermore, the magnitude of $a^{\parallel}_{j,\Gamma_\gamma}$ can deviate significantly from the other two diagonal entries because it can have pure spin contributions.

Group theory implies that the $\Gamma_{5/6}$ states cannot be coupled by operators transforming according to the E representation of C_{3v}, e.g. I_x, I_y. This follows from the requirement that in C_{3v} the spin-orbit operator part of H_{hf} has to transform according to the same basis vector of the same irrep as the corresponding nuclear spin operator, because H_{hf} as a whole has to transform according to A_1. On the other hand operators transforming according to E cannot couple states transforming according to $\Gamma_{5/6} = \Gamma_5 \oplus \Gamma_6$, as this combined irrep is not part of the direct product $E \otimes (\Gamma_5 \oplus \Gamma_6) = 2\Gamma_4 \not\supseteq \Gamma_5 \oplus \Gamma_6$. On the other hand the counterpart of I_z (transforming according to A_2) can couple these states. Finally, we stress that the pseudospin matrices are not angular momentum type operators and, therefore, $\sigma^x_{j,\Gamma_{5/6}}$ and $\sigma^z_{j,\Gamma_{5/6}}$ can in part transform according to A_2. For $\sigma^x_{j,\Gamma_{5/6}}$ the

relevant terms in the hyperfine Hamiltonian are $xzS_x + yzS_y$. As can be seen by the explicit calculation in Appendix B the contribution of these terms vanishes in the Γ_4 KDs. The difference between the Γ_4 KDs originating from the doublet and those from the singlet is due to the spin-orbit coupling leading to the pseudospin up state from the doublet transforming like the pseudospin down state from the singlet and vice versa.

We calculate the second order hyperfine interaction inside the KDs due to the interaction between KDs from the same orbital doublet with a Schrieffer-Wolff transformation [45], see Eq. (B17). We obtain the second-order correction

$$H^{\mathrm{hf},(2)}_{j,\Gamma_{5/6}} = -H^{\mathrm{hf},(2)}_{j,\Gamma_4} = a^{\mathrm{od}}_j \left(I^2 - I_z^2 - I_z\right), \tag{13}$$

for $j = 1, 2$ and $H^{\mathrm{hf},(2)}_{3,\Gamma_4} = 0$, with the defect-configuration dependent constant $a^{\mathrm{od}}_j = (a^2_{j,c} + a^2_{j,f})/\Delta^{\mathrm{so}}_j$. Combined with Eqs. (3), (7)–(9), and (11) this leads to the second order of the effective hyperfine Hamiltonians for the KDs

$$H_{i,\Gamma_\gamma} = H^{\mathrm{KD}}_{i,\Gamma_\gamma} + H^{\mathrm{hf}}_{i,\Gamma_\gamma} + H^{\mathrm{q}}_{i,\Gamma_\gamma} + H_{z,\mathrm{nuc}} + H^{\mathrm{hf},(2)}_{i,\Gamma_\gamma}. \tag{14}$$

We stress that the quadrupole Hamiltonian as well as the second order contribution of the hyperfine interaction is purely diagonal in the basis where z points along the crystal axis.

B. Comparison to Recent Experimental Results

We now compare our results to the recent measurements by Wolfowicz *et al.* [22], concentrating on the two ground state KDs. In Ref. [22] optically detected magnetic resonance of the ground states was performed, and to model the allowed resonant transition frequencies a model for the KDs with a form of the hyperfine coupling was used that deviates from our hyperfine Hamiltonian. The model $\sum_{k=x,y,z} a^k_{j,\Gamma_\gamma} \sigma^k_{j,\Gamma_\gamma} I_k/2$ was used for all KDs, including a tilt of the quantization axis of the pseudospin. Further technical details and resulting hyperfine coupling tensors for the KDs can be found in Appendix D. The above-mentioned measurement in combination with our theoretical model suggests that the lowest-energy ground states (GS1) correspond to $|1, \Gamma_4\rangle$ and GS2 to $|1, \Gamma_{5/6}\rangle$. The first point we want to highlight is that the measurement confirms that the $|1, \Gamma_{5/6}\rangle$ KD states do not couple via I_x, I_y and that a tilt of the pseudospin around the y axis corresponding to the coupling of I_z to $\sigma^x_{j,\Gamma_{5/6}}$ is found. We highlight that this artificial tilt of the quantization axis needs no further explanation in our theory where the $\sigma^x_{j,\Gamma_{5/6}} I_z$ coupling emerges naturally from the interplay of the crystal potential and the spin-orbit interaction.

The second point is that our model provides a resort to explain the measurements [22] for GS1 without the need for an anisotropy in the hyperfine coupling tensor in the plane perpendicular to the crystal axis. Our model Eq. (8) shows good agreement with the transition frequencies in Ref. [22], despite a deviation of two energies in some configurations for small magnetic fields. For larger magnetic fields ($B \geqslant$ 10 mT) indeed all energies are in agreement with the model in Ref. [22]. Not only does our model provide an explanation without the anisotropy, it furthermore reduces the number of free parameters. For the β configuration of the V defect in 4H-SiC we plot the comparison of the models in Fig. 3.

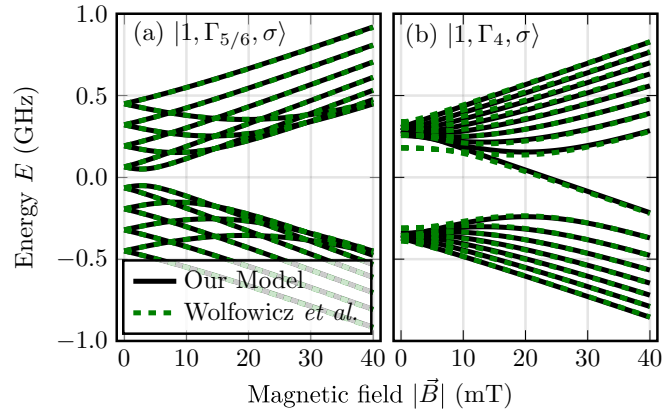

FIG. 3. Hyperfine energy levels without zero-field spin-orbit energies. For a V defect in the β configuration of 4H-SiC we compare our model (black solid lines), see Eq. (14), with the fitted model by Wolfowicz *et al.* [22] (green dashed lines). The fit for $\Gamma_{5/6}$ (a) of Ref. [22] is compatible with our model and the energy levels for the Γ_4 states (b) were calculated using a least squares fit for the eigenvalues of the models for magnetic fields between 2–45 mT with 200 data points. While there is a disagreement in the energy levels, the allowed transitions for magnetic microwave driving between the states are compatible with the experimental data. For the effective hyperfine constants we find $a^{\parallel}_{1,\Gamma_{5/6}}/h \approx 202.5$ MHz and $a^{\perp}_{1,\Gamma_{5/6}}/h \approx 158.2$ MHz, as well as $a^{\parallel}_{1,\Gamma_4}/h \approx -174.7 \pm 4.3$ MHz and $a^{\perp}_{1,\Gamma_4}/h \approx 149.5 \pm 4.2$ MHz, where the fit errors are due to the deviation at small magnetic fields. We additionally use $g_{1,\Gamma_4,\parallel} = 1.87$, $g_{1,\Gamma_{5/6},\parallel} = 2.035$, and $\mu_N g_N/h = -11.213$ MHz/T from Ref. [22].

Additionally, the measurement of β 6H-SiC in [22] includes all relevant electronic energy splittings allowing us to assign $|3, \Gamma_4\rangle$ to the lowest energy excited state, for which we find that the form of the hyperfine interaction of our theory agrees with their measurement.

C. Nuclear Quantum Memory

Finally we want to use the gained understanding of the effective hyperfine Hamiltonians within the KDs (14) [and Eqs. (7)–(9)] and investigate the consequences. The effective Hamiltonians can be block diagonalized in 2×2 blocks. In $\Gamma_{5/6}$ the KDs are mixed with each other but not with the nuclear spin, such that the resulting states are merely tilted around an axis perpendicular to the crystal axis. On the other hand, the Γ_4 KD electronic states are entangled with the nuclear spin, i.e.,

$$\begin{aligned} |i, \Gamma_4, +, m_I\rangle &= \cos(\phi_{i,\Gamma_4,m_I})\, |i, \Gamma_4, \uparrow\rangle\, |m_I\rangle \\ &+ \sin(\phi_{i,\Gamma_4,m_I})\, |i, \Gamma_4, \downarrow\rangle \begin{cases} |m_I - 1\rangle & \text{for} \quad i = 1, 2 \\ |m_I + 1\rangle & \text{for} \quad i = 3 \end{cases}, \end{aligned} \tag{15}$$

and similarly for the corresponding orthogonal states $|i, \Gamma_4, -, m_I \mp 1\rangle$. The hyperfine mixing angles ϕ_{i,Γ_4,m_I}, as well as the complete analytic diagonalization of the effective hyperfine Hamiltonian (14) including a static external magnetic field along the crystal axis can be found in Appendix C. In combination with the selection rules for the electronic states [30], the mixing leads to the allowed transitions between hyperfine states. Here we concentrate on a set of optical transitions under driving with an oscillatory

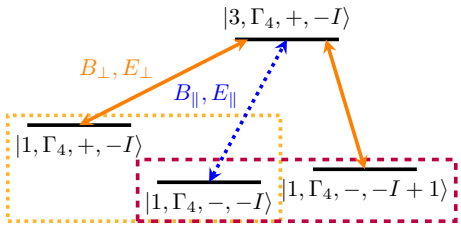

FIG. 4. Lambda (Λ) system to interface the electronic (pseudo) spin and nuclear spin states (orange arrows). Using the employed theory to find the hyperfine eigenstates for a static magnetic field parallel to the crystal axis as well as the selection rules for the spin-orbit eigenstates we obtain the allowed transitions between relevant states of different (pseudospin) KDs. The Lambda system can be used to transfer an electronic state $\alpha\,|j,\Gamma_4,-,-I\rangle+\beta\,|j,\Gamma_4,+,-I\rangle$ (yellow dotted frame) to a nuclear spin state (quantum memory, purple dashed frame) $\alpha\,|j,\Gamma_4,-,-I\rangle+\beta\,|j,\Gamma_4,-,-I+1\rangle$. The blue dotted (solid orange) line(s) corresponds to driving with a magnetic or electric field parallel (perpendicular) to the crystal axis.

electric field, $H_d=e\vec{r}\cdot\vec{E}_0\sin(\omega t)$, that can be used to transfer the pseudospin state of the ground-state KD $|1,\Gamma_4,\sigma\rangle$ to the nuclear spin and vice versa via a Lambda (Λ) system. We now consider the case where the electronic qubit is given by the states $|1\rangle$, $|0\rangle=|1,\Gamma_4,\pm,-I\rangle$. The $|0\rangle$ state is shared with the nuclear qubit where the excited state is given by $|1\rangle_{\rm nuc}=|1,\Gamma_4,-,-I+1\rangle$. While we choose a certain m_I here, the theory can be applied analogously to other encodings of the qubit. The states $m_I=\pm I$ have the benefit that they couple to fewer states.

Next, we outline the necessary details on how to transfer the state between the qubits as well as an experiment to measure the T_2^* time of the nuclear qubit while only directly controlling the electron. To achieve this we propose the use of the ancillary state $|3,\Gamma_4,+,-I\rangle$ that couples polarization dependently to the states of the electronic and nuclear qubit. This creates a Λ system that transfers the population from the $|1\rangle\leftrightarrow|1\rangle_{\rm nuc}$, see Fig. 4. The polarization dependence ensures that when driving the two photon process $|1\rangle\leftrightarrow|1\rangle_{\rm nuc}$ resonantly, no off-resonant transition to $|0\rangle$ is excited. Storing the state of the electronic qubit $\alpha\,|0\rangle+\beta\,|1\rangle$ to the nuclear qubit can be achieved by applying a π pulse to the Λ system (orange transitions in Fig. 4), resulting in the state $\alpha\,|0\rangle+\beta e^{i\psi_s}\,|1\rangle_{\rm nuc}$, where ψ_s is a known static phase gained during the pulse.

For a modified Ramsey experiment [14], one would first polarize the nuclear spin and prepare the electronic state $|0\rangle$. Now applying a $\pi/2$ pulse to the electronic qubit results in $(|0\rangle+|1\rangle)/\sqrt{2}$. This is followed by a π pulse via the optical Λ system to transfer the state to $(|0\rangle+e^{i\phi_s}\,|1\rangle_{\rm nuc})/\sqrt{2}$. During a (variable) free evolution of time T this state accumulates a further relative phase (different from the free evolution of the electronic qubit and independent of the initial state) given by $\psi=(E_{i,\Gamma_4,-,-I}-E_{i,\Gamma_4,-,-I+1})T/\hbar$, where the energies in terms of the model parameters and the static magnetic field strength can be found in Appendix C. Applying a second π pulse after the free evolution transfers the population back to the electronic qubit, that now has a different phase from the initially prepared state $\psi'=\psi+\delta\psi_s$ where $\delta\psi_s$ is another known static phase. Applying another electronic $\pi/2$ pulse leads to the state $(1-e^{i\psi'})/2\,|0\rangle+(1-e^{i\psi'})/2\,|1\rangle$ making the phase measurable via population measurements of the state $|0\rangle$ for different free evolution durations T. Due to decoherence the final state is not achieved perfectly; this is quantified by the inhomogeneous spin coherence time $T^*_{2,\rm nuc}$ that can be extracted from this kind of experiment [14].

Similarly, our effective theory shows that the hyperfine interaction opens the possibility to directly drive the pseudospin transition of the KDs for small magnetic fields due to the pseudospin tilt or the pseudospin nuclear entanglement; this was studied using a different framework by Gilardoni *et al.* [46]. Lastly, when the spin-orbit splitting is sufficiently small, the second order hyperfine interaction can enable optical driving inside the KDs by mixing the KDs of the same orbital doublet.

Finally we note that we mostly concentrated on the vanadium (V) defect, because it has a high isotopic purity, the transition line in the O band, as well as larger interest in the experimental community. Still, our theory is applicable to Mo as well, where the main differences are that only a fraction of the stable isotopes have nuclear spin and the (ground state) spin-orbit splitting is about twice the one in the corresponding V defect [23].

IV. CONCLUSIONS

In summary, we introduced a theory to describe the hyperfine interaction in TM defects in SiC having a single electron in a D shell. The theory yields insights into previous measurements and reduces the required number of fit parameters of the effective hyperfine coupling tensor. Combined with our previous work [30] the derived form of the coupling leads to selection rules between the hyperfine energy levels. We used these to construct a Λ system that can be exploited to create a nuclear spin quantum memory interfaced with the electronic qubit and proposed an experimental sequence to measure the T_2^* time of the nuclear qubit.

ACKNOWLEDGMENTS

We thank A. Csóré and A. Gali for useful discussions and acknowledge funding from the European Union's Horizon 2020 research and innovation programme under Grant Agreement No. 862721 (QuanTELCO).

APPENDIX A: ELECTRONIC HAMILTONIAN

The electronic Hamiltonian without the interaction with oscillating fields and the nuclear spin of the TM is [34]

$$H_{\rm el}=H_{\rm TM}+V_{\rm cr}+H_{\rm so}+H_z. \tag{A1}$$

The first term is the atomic Hamiltonian $H_{\rm TM}$ given by the kinetic energy of the active electron and the potential of the interaction of the active electron bound to the TM atom $V_{\rm TM}$ that localizes the active electron in the d orbital. The crystal potential $V_{\rm cr}$ describes the interaction with the lattice atoms and reduces the symmetry to C_{3v}. The symmetry reduction splits the five orbital levels into two doublets E and a singlet A_1, see Fig. 1(a).

The spin-orbit Hamiltonian $H_{\rm so}=\hbar/2m_e^2c^2\{\nabla[V_{\rm TM}+V_{\rm cr}]\times\vec{p}\}\cdot\vec{S}$, with the electron spin vector operator $\vec{S}=\vec{\sigma}/2$

in units of the reduced Planck constant $\hbar$ given by half the Pauli vector $\vec{\sigma}$, and the speed of light in vacuum c, describes the interaction of the orbital-angular momentum of the electron with the electron spin due to relativistic effects. This term splits each of the orbital doublets into two Kramers doublets, one transforming according to the irrep Γ_4 and one transforming according to the combination of irreps $\Gamma_{5/6} = \Gamma_5 \oplus \Gamma_6$.

The Zeeman Hamiltonian $H_z = \mu_B(g_s\vec{B}\cdot\vec{S} + \vec{B}\cdot\vec{L})$ describes the coupling to a static magnetic field which breaks time-reversal symmetry and thus energetically splits the KDs, here μ_B is the Bohr magneton, g_s the free electron g factor, and $\vec{L}$ the orbital angular momentum operator in units of $\hbar$. Because the coupling to electric fields is invariant under time inversion, electric fields cannot lift the degeneracy of the KDs, therefore we concentrate on static magnetic fields.

Due to several effects and because the precise form of V_{cr} is unknown we employ the Wigner-Eckart theorem to derive the most general symmetry-allowed form for the orbital operators. The application of the Wigner-Eckart theorem to the electronic Hamiltonian, the calculation of the block-diagonal effective Hamiltonian, as well as the derivation of the selection rules (for magnetic and electric dipole transitions) based on the form of the resulting electronic states can be found in Ref. [30]. The perturbative states are also shown in Eqs. (B5)–(B7), and the transformed effective electronic Hamiltonian in Eq. (B8).

APPENDIX B: DERIVATION OF H_{hf}

In this Appendix we show a more in-depth derivation of the general form of the hyperfine Hamiltonian of a spin-orbit coupled electron state in a D shell of a transition metal (TM) defect in a crystal environment with C_{3v} symmetry with the TM nuclear spin. We start by writing the hyperfine Hamiltonian with the nontrivial scalar products expanded

$$\begin{aligned} H_{\mathrm{hf}} = a_{\mathrm{FC}}\vec{S}\cdot\vec{I} - 3a\Bigg\{&\left[\left(-\frac{y^2-x^2}{2}S_x + xyS_y\right) + xzS_z + \frac{y^2+x^2}{2}S_x - S_x/3 + L_x/3\right]I_x \\ &+ \left[\left(\frac{y^2-x^2}{2}S_y + xyS_x\right) + yzS_z + \frac{y^2+x^2}{2}S_y - S_y/3 + L_y/3\right]I_y \\ &+ [(xzS_x + yzS_y) + z^2S_z - S_z/3 + L_z/3]I_z\Bigg\}, \end{aligned} \tag{B1}$$

where $(x, y, z)^T = \vec{r}/r$ are the direction vector components of the position $\vec{r}$ of the electron relative to the TM nucleus in the origin. In the appendices of Ref. [30] we discussed the application of the Wigner-Eckart theorem for the given symmetry in detail; analogously we use the eigenbasis of the crystal potential inside the subspace of d-orbital like states, made up of two doublets $|\pm\rangle_i$ transforming like the basis $|l=2, m=\pm1\rangle$ of E and given by admixtures of the states $|l=2, m\neq 0\rangle$ (and states that transform the same) as well as a singlet $|0\rangle = |l=2, m=0\rangle$ transforming according to A_1. For the hyperfine Hamiltonian (B1) the relevant operators are the square components kl with $k, l = x, y, z$ acting on the orbital states. These components can be mapped to operators that transform the same as x, y, z, implying a one-to-one correspondence of the application of the Wigner-Eckart theorem to the orbital terms of the electronic dipolar coupling $e\vec{E}\vec{r}$. In particular, z^2 and $(x^2+y^2)/2$ transform like z according to the irrep A_1, while $\{zx, zy\}$ and $\{(y^2-x^2)/2, xy\}$ transform like $\{x, y\}$ according to the irrep E. The orbital operators transforming like z have the form

$$\mathcal{Z}_{12}\left(\sum_{\sigma=\pm}|\sigma_1\rangle\langle\sigma_2| + \mathrm{H.c.}\right) + \sum_{i=1,2,3}\mathcal{Z}_{ii}P_i, \tag{B2}$$

where $P_j = |+_j\rangle\langle+_j| + |-_j\rangle\langle-_j|$ $(j=1,2)$ and $P_3 = |0\rangle\langle 0|$. The operators transforming like x have the form

$$\sum_{i,j=1,2}\mathcal{X}_{ij}(|+_i\rangle\langle-_j| + \mathrm{H.c.}) + \sum_{i=1,2}\mathcal{X}_{i3}(|+_i\rangle\langle 0| - |-_i\rangle\langle 0| + \mathrm{H.c.}) \tag{B3}$$

and the corresponding operator transforming like y

$$\sum_{i,j=1,2}\mathcal{X}_{ij}(\mathrm{i}\,|+_i\rangle\langle-_j| + \mathrm{H.c.}) + \sum_{i=1,2}\mathcal{X}_{i3}(\mathrm{i}\,|+_i\rangle\langle 0| + \mathrm{i}\,|-_i\rangle\langle 0| + \mathrm{H.c.}). \tag{B4}$$

While all operators transforming the same have these forms, the parameters $\mathcal{X}_{ij}$ and $\mathcal{Z}_{ij}$ vary. The $\vec{L}$ operators take the form discussed in Ref. [30].

Because the spin-orbit interaction is much larger than the hyperfine interaction, we first approximately diagonalize the spin-orbit Hamiltonian, using the first-order Schrieffer-Wolff transformation we derived in Ref. [30], given in terms of approximate eigenstates (rows of $1 - S_{\mathrm{so},1}$)

$$|i,\Gamma_{5/6},\sigma\rangle^{(1)} = |\sigma_i\rangle\,|\sigma\rangle + \sigma\frac{2\lambda_{\perp,12}r_{\parallel,12}}{(\epsilon_2-\epsilon_1)(g_s+2r_{\parallel,ii})}\,|-\sigma_i\rangle\,|-\sigma\rangle - \frac{(-1)^i\lambda_{\parallel,12}}{2(\epsilon_2-\epsilon_1)}\,|\sigma_{3-i}\rangle\,|\sigma\rangle - \frac{\sigma\lambda_{\perp,12}}{\epsilon_2-\epsilon_1}\,|-\sigma_{3-i}\rangle\,|-\sigma\rangle\,, \tag{B5}$$

$$|i,\Gamma_4,\sigma\rangle^{(1)} = |-\sigma_i\rangle\,|\sigma\rangle - \frac{(-1)^i\lambda_{\parallel,12}}{2(\epsilon_2-\epsilon_1)}\,|-\sigma_{3-i}\rangle\,|\sigma\rangle - \frac{\sigma\lambda_{\perp,i3}}{\epsilon_3-\epsilon_i}\,|0\rangle\,|-\sigma\rangle \text{ for } i<3 \quad \text{and} \tag{B6}$$

$$|3,\Gamma_4,\sigma\rangle^{(1)} = |0\rangle\,|\sigma\rangle + \frac{\sigma\lambda_{\perp,13}}{\epsilon_3-\epsilon_1}\,|\sigma_1\rangle\,|-\sigma\rangle + \frac{\sigma\lambda_{\perp,23}}{\epsilon_3-\epsilon_2}\,|\sigma_2\rangle\,|-\sigma\rangle\,, \tag{B7}$$

with $\sigma = \pm = \uparrow,\downarrow$, ϵ_j, ϵ_3 ($j = 1, 2$) the eigenvalues with the eigenvectors $|\pm_j\rangle$, $|0\rangle$ of the crystal potential, and $\lambda_{k,ij}$ the spin-orbit parameters.

With the Schrieffer-Wolff transformation we can approximate the Hamiltonian H [Eq. (1)] with an effective Hamiltonian $H_{\mathrm{eff}} = \sum_{i=1,2,3} P_i(H + [S_{\mathrm{so},1}, H])P_i = H_{\mathrm{el}}^{\mathrm{eff}} + H_d^{\mathrm{eff}} + H_{\mathrm{hf}}^{\mathrm{eff}} + H_q^{\mathrm{eff}} + H_{z,\mathrm{nuc}}$, with H_q^{eff} and $H_{z,\mathrm{nuc}}$ as discussed in the main text and selection rules between the orbital states under driving H_d^{eff} as discussed in Ref. [30]. Renaming the independent (combinations of) parameters we find

$$\begin{aligned} H_{\mathrm{el}}^{\mathrm{eff}} = \sum_{i,\Gamma_\gamma} H_{i,\Gamma_\gamma}^{\mathrm{KD}} + \sum_{j,\sigma}\frac{\mu_B}{2}[&g_{j,c}(\sigma B_x + iB_y) \\ &\times |j,\Gamma_{5/6},\sigma\rangle\langle j,\Gamma_4,\sigma| + g_{f,c}(B_x - \sigma iB_y) \\ &\times |j,\Gamma_{5/6},\sigma\rangle\langle j,\Gamma_4,-\sigma| + \mathrm{H.c.}] \end{aligned} \tag{B8}$$

with the KD Hamiltonians $H_{i,\Gamma_\gamma}^{\mathrm{KD}}$ from Eq. (3) of the main text and

$$\begin{aligned} H_{\mathrm{hf}}^{\mathrm{eff}} = \sum_{i,\Gamma_\gamma} H_{i,\Gamma_\gamma}^{\mathrm{hf}} + \sum_{j,\sigma} a_{j,f}[&(I_x - \sigma \mathrm{i} I_y) \\ &\times |j,\Gamma_{5/6},\sigma\rangle\langle j,\Gamma_4,-\sigma| + \mathrm{H.c.}]. + \sum_{j,\sigma} a_{j,c}[(\sigma I_x + \mathrm{i} I_y) \\ &\times |j,\Gamma_{5/6},\sigma\rangle\langle j,\Gamma_4,\sigma| + \mathrm{H.c.}] \end{aligned} \tag{B9}$$

with the diagonal blocks

$$H_{j,\Gamma_{5/6}}^{\mathrm{hf}} = \frac{1}{2}\left(a_{j,\Gamma_{5/6}}^{\parallel}\sigma_{j,\Gamma_{5/6}}^{z} + a_{j,\Gamma_{5/6}}^{\perp}\sigma_{j,\Gamma_{5/6}}^{x}\right)I_z, \tag{B10}$$

$$H_{j,\Gamma_4}^{\mathrm{hf}} = \frac{a_{j,\Gamma_4}^{\parallel}}{2}\sigma_{j,\Gamma_4}^{z}I_z + \frac{a_{j,\Gamma_4}^{\perp}}{2}\left(\sigma_{j,\Gamma_4}^{x}I_x - \sigma_{j,\Gamma_4}^{y}I_y\right), \tag{B11}$$

$$H_{3,\Gamma_4}^{\mathrm{hf}} = \frac{a_{3,\Gamma_4}^{\parallel}}{2}\sigma_{3,\Gamma_4}^{z}I_z + \frac{a_{3,\Gamma_4}^{\perp}}{2}\left(\sigma_{3,\Gamma_4}^{x}I_x + \sigma_{3,\Gamma_4}^{y}I_y\right), \tag{B12}$$

for $j = 1, 2$, and $\sigma_{i,\Gamma_\gamma}^{k}$ is the k Pauli matrix acting between the pseudospin states of the i,Γ_γ KD, i.e.,

$$\sigma_{i,\Gamma_\gamma}^{x} = |i,\Gamma_\gamma,\uparrow\rangle\langle i,\Gamma_\gamma,\downarrow| + \mathrm{H.c.}, \tag{B13}$$

$$\sigma_{i,\Gamma_\gamma}^{y} = -i\,|i,\Gamma_\gamma,\uparrow\rangle\langle i,\Gamma_\gamma,\downarrow| + \mathrm{H.c.}, \tag{B14}$$

$$\sigma_{i,\Gamma_\gamma}^{z} = |i,\Gamma_\gamma,\uparrow\rangle\langle i,\Gamma_\gamma,\uparrow| - |i,\Gamma_\gamma,\downarrow\rangle\langle i,\Gamma_\gamma,\downarrow|\,. \tag{B15}$$

Analogously we can write the above equations using coupling tensors $H_{i,\Gamma_\gamma}^{\mathrm{hf}} = \frac{1}{2}\vec{\sigma}_{i,\Gamma_\gamma}\cdot A_{i,\Gamma_\gamma}\cdot\vec{I}$, with

$$A_{j,\Gamma_{5/6}} = \begin{pmatrix} 0 & 0 & a_{j,\Gamma_{5/6}}^{\perp} \\ 0 & 0 & 0 \\ 0 & 0 & a_{j,\Gamma_{5/6}}^{\parallel} \end{pmatrix}, \quad A_{j,\Gamma_4} = \begin{pmatrix} a_{j,\Gamma_4}^{\perp} & 0 & 0 \\ 0 & -a_{j,\Gamma_4}^{\perp} & 0 \\ 0 & 0 & a_{j,\Gamma_4}^{\parallel} \end{pmatrix}, \quad A_{3,\Gamma_4} = \begin{pmatrix} a_{3,\Gamma_4}^{\perp} & 0 & 0 \\ 0 & a_{3,\Gamma_4}^{\perp} & 0 \\ 0 & 0 & a_{3,\Gamma_4}^{\parallel} \end{pmatrix}, \tag{B16}$$

and the Pauli vector $\vec{\sigma}_{i,\Gamma_\gamma} = (\sigma_{i,\Gamma_\gamma}^{x}, \sigma_{i,\Gamma_\gamma}^{y}, \sigma_{i,\Gamma_\gamma}^{z})^T$. We note that while we cannot estimate the magnitude of the different contributions to the hyperfine Hamiltonian within our theory, the main contribution is expected to be due to the anisotropic and orbital hyperfine interactions. In the leading order for these one would find $a_{j,\Gamma_{5/6}}^{\parallel} = -a_{j,\Gamma_4}^{\parallel}$ (for KDs with the same orbital origin, $j = 1, 2$) in agreement with the alternating signs found by the fit in Table I.

To take the block-off-diagonal part $H_{\mathrm{hf,od}}$ of (B9) into account, we apply a second Schrieffer-Wolff transformation. Here, the unperturbed Hamiltonian $H_0 = \sum_{i,\Gamma_\gamma} E_{i,\Gamma_\gamma}P_{i,\Gamma_\gamma}$ becomes perturbed inside the KDs by $V_d = H_{\mathrm{hf,bd}} + H_{z,\mathrm{nuc}} + \sum_{i,\Gamma_\gamma}\mu_B g_\parallel B_z\sigma_{i,\Gamma_\gamma}^{z}/2$ and between KDs with the same orbital origin by $H_{\mathrm{hf,od}}$, leading to the first-order Schrieffer-Wolff transformation

$$S_1 = \sum_{j,\sigma}\frac{1}{\Delta_j^{\mathrm{so}}}(a_{j,c}\sigma\,|j,\Gamma_{5/6},\sigma\rangle\langle j,\Gamma_4,\sigma|\,I_\sigma + a_{j,f}\,|j,\Gamma_{5/6},\sigma\rangle\langle j,\Gamma_4,-\sigma|\,I_{-\sigma} - \mathrm{H.c.}), \tag{B17}$$

and the new effective Hamiltonian $\tilde{H} = H_0 + V_{\mathrm{d}} + [S_1, H_{\mathrm{hf,od}}]/2$. After projection into one of the KDs, the effective interaction term becomes $H_{i,\Gamma_\gamma}^{\mathrm{hf},(2)} = P_{i,\Gamma_\gamma}[S_1, H_{\mathrm{hf,od}}]P_{i,\Gamma_\gamma}/2$.

TABLE I. Hyperfine tensors for our model calculated using the fit values of Wolfowicz *et al.* [22]; the defect type assignment in brackets is according to the *ab initio* results by A. Csóré *et al.* We omit the errors for the $\Gamma_{5/6}$, because we can directly calculate [see Eq. (D1)] the values from their fit data such that there is no additional error due to fitting. Furthermore we show the values of the crystal splitting Δ_{cr} between the lowest energy ground and excited state, as well as the spin-orbit splitting between the two ground states as determined in Ref. [22] (measurement error $\approx$1 GHz for both Δ_2^{so} and Δ_{cr}).

Irrep	Crystal	Defect type	$a^{\perp}_{1,\Gamma_\gamma}/h$ (MHz)	$a^{\parallel}_{1,\Gamma_\gamma}/h$ (MHz)	Δ_{cr}/h (THz) [22]	Δ_1^{so}/h (GHz) [22]
Γ_4	4H-SiC	α (k)	165.1 ± 1.7	-232.0 ± 3.9	234.4	529
Γ_4	4H-SiC	β (h)	149.5 ± 4.2	-174.7 ± 4.3	224.5	43
Γ_4	6H-SiC	α (k_2)	165.1 ± 1.6	-232.0 ± 3.6	229.1	524
Γ_4	6H-SiC	β (k_1)	141.6 ± 2.4	-171.2 ± 2.1	221.8	25
Γ_4	6H-SiC	γ (h)	147.3 ± 14.5	-175.4 ± 13.6	216.0	16
$\Gamma_{5/6}$	4H-SiC	β (h)	202.5	158.2		
$\Gamma_{5/6}$	6H-SiC	β (k_1)	197.6	165.8		
$\Gamma_{5/6}$	6H-SiC	γ (h)	205.9	166.8		

APPENDIX C: DIAGONALIZATION FOR A MAGNETIC FIELD ALONG THE CRYSTAL AXIS

In this Appendix we diagonalize the effective hyperfine Hamiltonian of the KDs, Eq. (14). The effective hyperfine Hamiltonians can be decomposed into 2×2 blocks for a magnetic field $\vec{B}$ along the crystal axis. For the $j, \Gamma_{5/6}$ states the blocks are spanned by $|j, \Gamma_{5/6}, \uparrow\rangle |m_I\rangle$, $|j, \Gamma_{5/6}, \downarrow\rangle |m_I\rangle$, for the $j = 1, 2, \Gamma_4$ states by $|j, \Gamma_4, \uparrow\rangle |m_I\rangle$, $|j, \Gamma_4, \downarrow\rangle |m_I - 1\rangle$ (the states $|j, \Gamma_4, \uparrow\rangle |-I\rangle$, $|j, \Gamma_4, \downarrow\rangle |I\rangle$ are already diagonal), and for 3, Γ_4 states by $|3, \Gamma_4, \uparrow\rangle |m_I\rangle$, $|3, \Gamma_4, \downarrow\rangle |m_I + 1\rangle$ (the states $|3, \Gamma_4, \uparrow\rangle |I\rangle$, $|3, \Gamma_4, \downarrow\rangle |-I\rangle$ are already diagonal). We can diagonalize the nondiagonal blocks with the transformations

$$T_{j,\Gamma_{5/6},m_I} = \exp\big(-\mathrm{i}\phi_{j,\Gamma_{5/6},m_I}\sigma^{y}_{j,\Gamma_{5/6}}\big)\,|m_I\rangle\,\langle m_I|\,, \qquad \text{with } \tan\big(2\phi_{j,\Gamma_{5/6},m_I}\big) = \frac{a^{\perp}_{j,\Gamma_{5/6}} m_I}{\mu_B B g^{\parallel}_{j,\Gamma_{5/6}} + a^{\parallel}_{j,\Gamma_{5/6}} m_I}; \tag{C1}$$

$$T_{j,\Gamma_4,m_I} = \exp\big[-i\phi_{j,\Gamma_4,m_I}(-i\,|j,\Gamma_4,\uparrow\rangle\,|m_I\rangle\,\langle m_I - 1|\,\langle j,\Gamma_4,\downarrow| + \text{H.c.})\big],$$

$$\text{with } \tan 2\phi_{j,\Gamma_4,m_I} = \frac{a^{\perp}_{j,\Gamma_4}\sqrt{I(I+1) - m_I(m_I-1)}}{\mu_B g^{\parallel}_{j,\Gamma_4} B + \big(a^{\parallel}_{j,\Gamma_4} + 6q_{j,\Gamma_4}\big)(m_I - 1/2) + \mu_N g_N B + a^{\mathrm{od}}_j 2m_I}; \tag{C2}$$

$$T_{3,\Gamma_4,m_I} = \exp\big[-i\phi_{3,\Gamma_4,m_I}(-i\,|3,\Gamma_4,\uparrow\rangle\,|m_I\rangle\,\langle m_I + 1|\,\langle 3,\Gamma_4,\downarrow| + \text{H.c.})\big],$$

$$\text{with } \tan 2\phi_{3,\Gamma_4,m_I} = \frac{a^{\perp}_{3,\Gamma_4}\sqrt{I(I+1) - m_I(m_I+1)}}{\mu_B g^{\parallel}_{3,\Gamma_4} B + \big(a^{\parallel}_{3,\Gamma_4} + 6q_{3,\Gamma_4}\big)(m_I + 1/2) - \mu_N g_N B}. \tag{C3}$$

The corresponding eigenvalues are

$$E_{j,\Gamma_{5/6},\pm,m_I} = E_{j,\Gamma_{5/6}} \pm \frac{\mu_B B g^{\parallel}_{j,\Gamma_{5/6}} + a^{\parallel}_{j,\Gamma_{5/6}} m_I}{2\,|\cos 2\phi_{j,\Gamma_{5/6},m_I}|} + \mu_N g_N m_I B + q_{j,\Gamma_{5/6}}\big[3m_I^2 - I(I+1)\big] + a^{\mathrm{od}}_j[I(I+1) - m_I(m_I+1)], \tag{C4}$$

$$E_{j,\Gamma_4,\pm,m_I\pm 1/2-1/2} = E_{j,\Gamma_4} + \frac{a^{\parallel}_{j,\Gamma_4}}{4} \pm \frac{\mu_B g^{\parallel}_{j,\Gamma_4} B + \big(a^{\parallel}_{j,\Gamma_4} + 6q_{j,\Gamma_4}\big)(m_I - 1/2) + \mu_N g_N B + a^{\mathrm{od}}_j 2m_I}{2\,|\cos 2\phi_{j,\Gamma_4,m_I}|}$$
$$+ \mu_N g_N B(m_I - 1/2) + q_{j,\Gamma_4}\left[3\left(m_I^2 - m_I + \frac{1}{2}\right) - I(I+1)\right] + a^{\mathrm{od}}_j\big[m_I^2 - I(I+1)\big], \tag{C5}$$

$$E_{3,\Gamma_4,\pm,m_I\mp 1/2+1/2} = E_{3,\Gamma_4} - \frac{a^{\parallel}_{3,\Gamma_4}}{4} \pm \frac{\mu_B g^{\parallel}_{3,\Gamma_4} B + \big(a^{\parallel}_{3,\Gamma_4} + 6q_{3,\Gamma_4}\big)(m_I + 1/2) - \mu_N g_N B}{2\,|\cos 2\phi_{3,\Gamma_4,m_I}|}$$
$$+ \mu_N g_N B(m_I + 1/2) + q_{j,\Gamma_4}\left[3\left(m_I^2 + m_I + \frac{1}{2}\right) - I(I+1)\right], \tag{C6}$$

where we use the contribution of the wave function proportional to $\cos(\phi_{i,\Gamma_\gamma,m_I})$ to label the energies.

APPENDIX D: HYPERFINE TENSORS FOR EXPERIMENTAL DATA FROM WOLFOWICZ *et al.*

We compared our model briefly to data by Wolfowicz *et al.* [22] in the main text; here we provide Table I with the least square fits for Γ_4 defects to translate their model to our model as well as the parameters for $\Gamma_{5/6}$ defects that can be calculated directly using their principal axis tilt θ and A_{ZZ} ($a^{z}_{j,\Gamma_{5/6}}$ with $j = 1, 2$ in the notation of the main text) value,

$$a^{\perp}_{j,\Gamma_\gamma} = \sin(\theta) A_{ZZ}, \qquad a^{\parallel}_{j,\Gamma_\gamma} = \cos(\theta) A_{ZZ}. \tag{D1}$$

The fit with the worst agreement is for the γ site of 6H-SiC, we want to stress that in this case the data provided in the Supplemental Material in Ref. [22] seems to be not described perfectly by their model, too. As this defect configuration also has the smallest Δ_1^{so} it would be reasonable to include the second order hyperfine energy correction when fitting to the raw data. The signs in the table carry no physical meaning here, because we did not choose a particular orientation of the z axis, i.e., we do not show the stacking order of the crystal with regard to the direction of the z axis and inverting the magnetic field $B_z \rightarrow -B_z$ corresponds to changing the sign of $a^{\parallel}_{j,\Gamma_\gamma}$ in the isolatet KD hyperfine energy lines. The sign of the off-diagonal elements in comparison to the diagonal elements has no effect on the energy levels used in the fit. The magnitudes of the contributions of the crystal field and the ground-state spin-orbit splitting for the different defect configurations are included in Table I.

Due to availability of measurements of the hyperfine tensor components for V we concentrated on this defect, but for completeness we note that the crystal field splitting for measurements of Mo (h site in 6H-SiC) [21] with about 267.4 THz is of similar magnitude as for the V defects and the spin-orbit coupling is larger than for V. According to Ref. [23] (where the same site is assigned differently, as the k_2 site) it has a spin-orbit splitting of about 1106.05 GHz, about twice the splitting in V. With this, we see that the arguments given based on the spin-orbit structure in the main text hold for V as well as Mo.

[1] H. J. Kimble, The quantum internet, Nature (London) **453**, 1023 (2008).

[2] I. Aharonovich, D. Englund, and M. Toth, Solid-state single-photon emitters, Nat. Photonics **10**, 631 (2016).

[3] K. Heshami, D. G. England, P. C. Humphreys, P. J. Bustard, V. M. Acosta, J. Nunn, and B. J. Sussman, Quantum memories: Emerging applications and recent advances, J. Mod. Opt. **63**, 2005 (2016).

[4] D. Awschalom, K. K. Berggren, H. Bernien, S. Bhave, L. D. Carr, P. Davids, S. E. Economou, D. Englund, A. Faraon, M. Fejer, S. Guha, M. V. Gustafsson, E. Hu, L. Jiang, J. Kim, B. Korzh, P. Kumar, P. G. Kwiat, M. Lončar, M. D. Lukin *et al.*, Development of quantum interconnects (quics) for next-generation information technologies, PRX Quantum **2**, 017002 (2021).

[5] A. A. Clerk, K. W. Lehnert, P. Bertet, J. R. Petta, and Y. Nakamura, Hybrid quantum systems with circuit quantum electrodynamics, Nat. Phys. **16**, 257 (2020).

[6] D. S. Smirnov, T. S. Shamirzaev, D. R. Yakovlev, and M. Bayer, Dynamic Polarization of Electron Spins Interacting with Nuclei in Semiconductor Nanostructures, Phys. Rev. Lett. **125**, 156801 (2020).

[7] G. Burkard, M. J. Gullans, X. Mi, and J. R. Petta, Superconductor–semiconductor hybrid-circuit quantum electrodynamics, Nat. Rev. Phys. **2**, 129 (2020).

[8] X.-F. He, N. B. Manson, and P. T. H. Fisk, Paramagnetic resonance of photoexcited N-V defects in diamond. I. level anticrossing in the ^{3}A ground state, Phys. Rev. B **47**, 8809 (1993).

[9] T. Gaebel, M. Domhan, I. Popa, C. Wittmann, P. Neumann, F. Jelezko, J. R. Rabeau, N. Stavrias, A. D. Greentree, S. Prawer, J. Meijer, J. Twamley, P. R. Hemmer, and J. Wrachtrup, Room-temperature coherent coupling of single spins in diamond, Nat. Phys. **2**, 408 (2006).

[10] L. Childress, M. V. G. Dutt, J. M. Taylor, A. S. Zibrov, F. Jelezko, J. Wrachtrup, P. R. Hemmer, and M. D. Lukin, Coherent dynamics of coupled electron and nuclear spin qubits in diamond, Science **314**, 281 (2006).

[11] A. Gali, M. Fyta, and E. Kaxiras, *Ab initio* supercell calculations on nitrogen-vacancy center in diamond: Electronic structure and hyperfine tensors, Phys. Rev. B **77**, 155206 (2008).

[12] S. Felton, A. M. Edmonds, M. E. Newton, P. M. Martineau, D. Fisher, D. J. Twitchen, and J. M. Baker, Hyperfine interaction in the ground state of the negatively charged nitrogen vacancy center in diamond, Phys. Rev. B **79**, 075203 (2009).

[13] J. R. Maze, A. Gali, E. Togan, Y. Chu, A. Trifonov, E. Kaxiras, and M. D. Lukin, Properties of nitrogen-vacancy centers in diamond: The group theoretic approach, New J. Phys. **13**, 025025 (2011).

[14] G. D. Fuchs, G. Burkard, P. V. Klimov, and D. D. Awschalom, A quantum memory intrinsic to single nitrogen–vacancy centres in diamond, Nat. Phys. **7**, 789 (2011).

[15] L. Busaite, R. Lazda, A. Berzins, M. Auzinsh, R. Ferber, and F. Gahbauer, Dynamic ^{14}N nuclear spin polarization in nitrogen-vacancy centers in diamond, Phys. Rev. B **102**, 224101 (2020).

[16] S. S. Hegde, J. Zhang, and D. Suter, Efficient Quantum Gates for Individual Nuclear Spin Qubits by Indirect Control, Phys. Rev. Lett. **124**, 220501 (2020).

[17] M. W. Doherty, N. B. Manson, P. Delaney, F. Jelezko, J. Wrachtrup, and L. C. L. Hollenberg, The nitrogen-vacancy colour centre in diamond, Phys. Rep. **528**, 1 (2013).

[18] D. Suter and F. Jelezko, Single-spin magnetic resonance in the nitrogen-vacancy center of diamond, Prog. Nucl. Magn. Reson. Spectrosc. **98-99**, 50 (2017).

[19] T. Bosma, G. J. J. Lof, C. M. Gilardoni, O. V. Zwier, F. Hendriks, B. Magnusson, A. Ellison, A. Gällström, I. G. Ivanov, N. T. Son, R. W. A. Havenith, and C. H. van der Wal, Identification and tunable optical coherent control of transition-metal spins in silicon carbide, npj Quantum Inf. **4**, 48 (2018).

[20] L. Spindlberger, A. Csóré, G. Thiering, S. Putz, R. Karhu, J. U. Hassan, N. T. Son, T. Fromherz, A. Gali, and M. Trupke, Optical Properties of Vanadium in 4*H* Silicon Carbide for Quantum Technology, Phys. Rev. Applied **12**, 014015 (2019).

[21] C. M. Gilardoni, T. Bosma, D. van Hien, F. Hendriks, B. Magnusson, A. Ellison, I. G. Ivanov, N. T. Son, and C. H. van der Wal, Spin-relaxation times exceeding seconds for color centers with strong spin–orbit coupling in SiC, New J. Phys. **22**, 103051 (2020).

[22] G. Wolfowicz, C. P. Anderson, B. Diler, O. G. Poluektov, F. J. Heremans, and D. D. Awschalom, Vanadium spin qubits as telecom quantum emitters in silicon carbide, Sci. Adv. **6**, eaaz1192 (2020).

[23] A. Csóré and A. Gali, *Ab initio* determination of pseudospin for paramagnetic defects in SiC, Phys. Rev. B **102**, 241201(R) (2020).

[24] B. Kaufmann, A. Dörnen, and F. S. Ham, Crystal-field model of vanadium in 6H silicon carbide, Phys. Rev. B **55**, 13009 (1997).

[25] J. Baur, M. Kunzer, and J. Schneider, Transition metals in SiC polytypes, as studied by magnetic resonance techniques, Phys. Status Solidi (a) **162**, 153 (1997).

[26] J. Meija, T. B. Coplen, M. Berglund, W. A. Brand, P. D. Bièvre, M. Gröning, N. E. Holden, J. Irrgeher, R. D. Loss, T. Walczyk, and T. Prohaska, Isotopic compositions of the elements 2013 (IUPAC technical report), Pure Appl. Chem. **88**, 293 (2016).

[27] M. Barbouche, R. B. Zaghouani, N. Benammar, V. Aglieri, M. Mosca, R. Macaluso, K. Khirouni, and H. Ezzaouia, New process of silicon carbide purification intended for silicon passivation, Superlattices Microstruct. **101**, 512 (2017).

[28] V. Mazzocchi, P. Sennikov, A. Bulanov, M. Churbanov, B. Bertrand, L. Hutin, J. Barnes, M. Drozdov, J. Hartmann, and M. Sanquer, 99.992% 28 si cvd-grown epilayer on 300 mm substrates for large scale integration of silicon spin qubits, J. Cryst. Growth **509**, 1 (2019).

[29] G. Audi, O. Bersillon, J. Blachot, and A. Wapstra, The NUBASE evaluation of nuclear and decay properties, Nucl. Phys. A **729**, 3 (2003).

[30] B. Tissot and G. Burkard, Spin structure and resonant driving of spin-1/2 defects in SiC, Phys. Rev. B **103**, 064106 (2021).

[31] F. S. Ham, Dynamical Jahn-Teller effect in paramagnetic resonance spectra: Orbital reduction factors and partial quenching of spin-orbit interaction, Phys. Rev. **138**, A1727 (1965).

[32] F. S. Ham, Effect of linear Jahn-Teller coupling on paramagnetic resonance in a ^2E state, Phys. Rev. **166**, 307 (1968).

[33] J. F. Cornwell, *Group Theory in Physics: An Introduction* (Academic Press, San Diego, Calif, 1997).

[34] M. S. Dresselhaus, G. Dresselhaus, and A. Jorio, *Group Theory: Application to the Physics of Condensed Matter* (Springer-Verlag, Berlin, 2010).

[35] E. I. Gryncharova and V. I. Perel', Relaxation of nuclear spins interacting with holes in semiconductors, Sov. Phys. Semicond. **11**, 997 (1977).

[36] A. Abragam, *The Principles of Nuclear Magnetism* (Oxford University Press, Oxford, 1961).

[37] C. Slichter, *Principles of Magnetic Resonance* (Springer, Berlin, Heidelberg, 1990).

[38] W. A. Coish and J. Baugh, Nuclear spins in nanostructures, Phys. Status Solidi (b) **246**, 2203 (2009).

[39] M. L. Munzarová, P. Kubáček, and M. Kaupp, Mechanisms of EPR hyperfine coupling in transition metal complexes, J. Am. Chem. Soc. **122**, 11900 (2000).

[40] G. Micera and E. Garribba, Is the spin-orbit coupling important in the prediction of the ^{51}V hyperfine coupling constants of $V^{VI}O^{2+}$ species? ORCA versus gaussian performance and biological applications, J. Comput. Chem. **32**, 2822 (2011).

[41] J. Vícha, M. Straka, M. L. Munzarová, and R. Marek, Mechanism of spin-orbit effects on the ligand NMR chemical shift in transition-metal complexes: Linking NMR to EPR, J. Chem. Theory Comput. **10**, 1489 (2014).

[42] S. Gohr, P. Hrobárik, M. Repiský, S. Komorovský, K. Ruud, and M. Kaupp, Four-component relativistic density functional theory calculations of EPR g- and hyperfine-coupling tensors using hybrid functionals: Validation on transition-metal complexes with large tensor anisotropies and higher-order spin-orbit effects, J. Phys. Chem. A **119**, 12892 (2015).

[43] N. Stone, Table of nuclear magnetic dipole and electric quadrupole moments, At. Data Nucl. Data Tables **90**, 75 (2005).

[44] I. D. Avdeev and D. S. Smirnov, Hyperfine interaction in atomically thin transition metal dichalcogenides, Nanoscale Adv. **1**, 2624 (2019).

[45] S. Bravyi, D. P. DiVincenzo, and D. Loss, Schrieffer-Wolff transformation for quantum many-body systems, Ann. Phys. **326**, 2793 (2011).

[46] C. M. Gilardoni, I. Ion, F. Hendriks, M. Trupke, and C. H. van der Wal, Hyperfine-mediated transitions between electronic spin-1/2 levels of transition metal defects in SiC, New J. Phys. (to be published).